The dynamic and thermodynamic processes dominating the reduction of global land monsoon precipitation driven by anthropogenic aerosols emission

Article

Accepted Version

The dynamic and thermodynamic processes dominating the reduction of global land monsoon precipitation driven by anthropogenic aerosols emission

Tianjun ZHOU[1,2,3]*, Wenxia ZHANG[1,3], Lixia ZHANG[1,2], Xuebin ZHANG[4], Yun QIAN[5], Dongdong PENG[6, 1], Shuangmei MA[1,3], Buwen DONG[7]

[1]State Key Laboratory of Numerical Modeling for Atmospheric Sciences and Geophysical Fluid Dynamics, Institute of Atmospheric Physics, Chinese Academy of Sciences, Beijing 100029, China.

[2] CAS Center for Excellence in Tibetan Plateau Earth Sciences, Chinese Academy of Sciences (CAS), Beijing 100101, China.

[3]University of Chinese Academy of Sciences, Beijing 100049, China.

[4]Environment and Climate Change Canada, 4905 Dufferin Street, Toronto, ON, Canada.

[5]Atmospheric Science and Global Change Division, Pacific Northwest National Laboratory, Richland, Washington 99352, USA.

[6]Institute of Tropical and Marine Meteorology, China Meteorological Administration, Guangzhou 510640, China

[7]National Centre for Atmospheric Science, Department of Meteorology, University of Reading, Reading RG6 6BB, UK.

*Corresponding author (email: zhoutj@lasg.iap.ac.cn)

Abstract

Changes in monsoon precipitation have profound social and economic impacts as more than two-thirds of the world's population lives in monsoon regions. Observations show a significant reduction in global land monsoon precipitation during the second half of the 20th century. Understanding the cause of this change, especially possible anthropogenic origins, is important. Here, we compare observed changes in global land monsoon precipitation during 1948~2005 with those simulated by 5 global climate models participating in the Coupled Model Inter-comparison Project-phase 5 (CMIP5) under different external forcings. We show that the observed drying trend is consistent with the model simulated response to anthropogenic forcing and to anthropogenic aerosol forcing in particular. We apply the optimal fingerprinting method to quantify anthropogenic influences on precipitation and find that anthropogenic aerosols may have contributed to 102% (62~144% for the 5~95% confidence interval) of the observed decrease in global land monsoon precipitation. A moisture budget analysis indicates that the reduction in precipitation results from reduced vertical moisture advection in response to aerosol forcing. Since much of the monsoon regions, such as India and China, have been experiencing rapid developments with increasing aerosol emissions in the past decedes, our results imply a further reduction in monsoon precipitation in these regions in the future if effective mitigations to reduce aerosol emissions are not deployed. The observed decline of aerosol emission in China since 2006 helps to alleviate the reducing trend of monsoon precipiptaion.

Key words: global monsoon, detection, attribution, aerosol forcing

1 Introduction

Changes in monsoon precipitation are of great scientific importance and significant societal concern owing to the facts that monsoon affects a large population. The global monsoon system includes Asian-Australia monsoon (South Asian, East Asian, Northwestern Pacfic and Australian monsoons), African monsoon (North African and South African monsoons) and American monsoon (North American and South American monsoons). A number of observational studies have reported a significant drying trend in the global monsoon precipitation during the second half of the 20th century (Wang and Ding, 2006; Zhou et al., 2008a; Zhang and Zhou, 2011; Polson et al., 2014). Understanding the causes of these changes is vital to infrastructural planning, water resource management, and sustainable development.

The changes of global monsoon are modulated by several factors. Different factors including the greenhouse gases (GHGs) (Kitoh et al., 2013; Song et al., 2014; Chen and Zhou, 2015), anthropogenic aerosols (AAs) (Held et al., 2005; Lau et al., 2006; Meehl et al., 2008; Bollasina et al., 2011; Qian et al., 2011; Jiang et al., 2013, 2015; Guo et al., 2013; Wu et al., 2013; Polson et al., 2014; Song et al., 2014; Li et al., 2016; Zhang et al., 2018), and natural internal variability of the climate system, such as the Inter-decadal Pacific Oscillation (IPO) (Zhu and Yang, 2003; Yang et al., 2004; Zhou et al., 2008b; Li et al., 2010; Wang et al., 2012; Huang et al., 2020), have been proposed to explain the observed reduction in monsoon precipitation. The impact of individual factors is regional dependent, including the sign and magnitude of impact (Polson et al., 2014; Pascale et al., 2017).

Greenhouse gases can modulate monsoon circulations in two ways. On the one hand, the greenhouse gases can intensify the land-sea thermal contrast and the hemispheric thermal contrast to enhance East Asian summer monsoon. On the other hand, it would broaden the descent branch of Hadley circulation and weaken Walker circulation by increasing the atmpsheric stability, weakening the monsoon circulation. Competetion between the two mechanisms leads to a slightly increase in East Asian summer monsoon (Song et al., 2014; Lau and Kim, 2017). Greenhouse gases may also result in uneven warming of sea surface temperature, thus modulating regional monsoon circulations. In the late half of 20^{th} century, the warming in the tropical Northwestern Pacific has led to anmolaous circulation anomalies at lower level and transported more dry air to South Asia, resulting in reduced rainfall over South Asia (Annamalai et al., 2013).

The impact of anthropogenic aerosol forcing is more complex. Although the impact of anthropogenic aerosols on the decline of northern hemispheric monsoon precipitation in the past decades has been detected (Polson et al., 2014), there is no consensus on the dominant dynamical processes. In the East Asian summer monsoon season, aersols could reduce the land-sea thermal contrast and increase atmospheric stability, thus weakening the summer monsoon circulation (Song et al., 2014). In South Asia, aerosols could reduce the income shortwave radition, cool the surface, reduce local evaporation and water vapor content. It could also increase the atmospheric stability and reduce the hemispheric thermal contrast, resulting in a weaker South Asian summer monsoon and less precipitation (Lau et al., 2006; Bollasina et al., 2011; Salzmann et al., 2014; Guo et al., 2013). In addition, different types of aersols extert different impacts (e.g., the local and remote forcing of aerosols) on regional monsoons (Jiang et al., 2013; Dong et al., 2016; Wang et al., 2017). Recent studies documented that the land use and land cover changes in the recent decades can alter the albedo and evaportation to reduce monsoon precipitation (Krishnan et al., 2016; Paul et al., 2016).

In addition to the external forcings, the monsoon system is influenced by internal variability of the climate. On the decadal to inter-decadal time scales, the Atlandtic Multi-decadal Oscillation (AMO) and Pacific Decadal Oscillation (PDO/IPO) can extert impacts on regional to hemespheric monsoon precipitation changes through modulating the Walker and Hadley circulation (Zhou et al., 2008b; Li et al., 2010; Krishnamurthy and Krishnamurthy, 2014; Wang et al., 2013; Jiang and Zhou, 2019). Thus, the changes in the global monsoon system are the compound results of external forcings and interal variability. Due to the complexity of the global monsoon system, it is still unclear about the main cause and mechanisms behind the declined precipitation in global land monsoon since the 1950s.

Here, we consider these multiple factors in a unified framework to determine the dominant factor, quantify its contribution, and physically understand how competing factors influence the observed changes from a global perspective. To understand the potential relative contributions of natural (solar variations and volcanoes) and anthropogenic (well-mixed GHGs, aerosols) forcings to the drying trend in global land monsoon domains, ensemble simulations from 5 state-of-the-art coupled climate system models are used to attribute the observed long-term trend. The rigorous "optimal fingerprinting" method is used to examine whether the anthropogenic influence is detectable and attributable in the historical changes of global land monsoon precipitation. A moisture budget analysis is then performed to understand the physical processes that dominate the detected historical changes. We show evidences that the drying trend in monsoon precipitation results from the reduction in vertical moisture advection due to aerosol forcing, the underlying physical processes include a thermodynamic effect due to the reduction in atmospheric humidity and a dynamic effect due to weakening of the land-sea thermal contrast and thus monsoon circulation.

The remainder of the paper is organized as following. The data and mtethods are decrisbed in section 2. The analysis results are presented in section 3. Section 4 summarizes the major findings along with a discussion.

2 Data and Methods

2.1 Data

Multiple observational datasets are compared to better account for uncertainties in the observations. The six observational monthly precipitation datasets used in our analysis include Climate Research Unit TS V4.01 (CRU) (Harris et al., 2014), Global Precipitation Climatology Center Full V6 (GPCC) (Schneider et al., 2014), University of Delaware precipitation V4.01 (Delaware) (Willmontt et al., 2001), NOAA's Precipitation Reconstruction over Land (PREC/L) (Chen et al., 2002), Variability Analysis of Surface Climate Observations (VASClimO, V1.1) from 1950~2005 (Beck et al., 2005); and GHCN V2 (Peterson et al., 1997). All data sets are regridded to a common 2.5° x 2.5° resolution. We focus on the common time period of 1948~2005. An ensemble average of CRU, GPCC, Delaware, PREC/L and GHCN data is used in our analysis. The precipitation dataset from VASClimO is not employed when calculating the ensemble mean due to a shorter time coverage, we note that it also shows a similar trend over the common time period of 1951~2000 (Fig. 1).

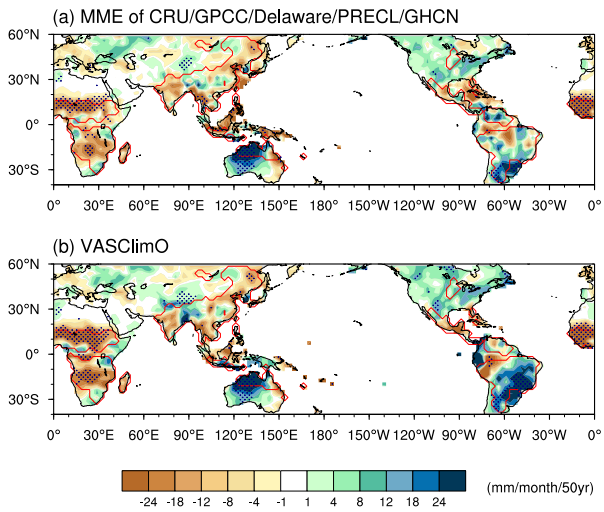

Figure 1. The spatial distributions of the linear trends in the local summer precipitation during 1951~2000 derived from (a) the multi-observation ensemble mean of CRU, GPCC, University of Delaware, PREC/L, and GHCN, and (b) VASClimO. Stippling indicates the 5% significance level. Red lines denote the global land monsoon regions.

We analyze 5 CMIP5 models (i.e., CanESM2, CSIRO-Mk3-6-0, GFDL-CM3, GISS-E2-H, and GISS-E2-R), which provide separate forcing simulations under greenhouse gases, anthropogenic aerosols, and natural forcing (NAT) forcings only, meanwhile each individual forcing simulation includes multiple realizations (Table1; Taylor et al., 2012). The 5 models provide a total of 101 simulations, including 32 historical, 23 historical GHG, 23 historical anthropogenic aerosols, and 23 historical natural experiments. The historical simulations (*ALL-forcing*) are forced by both natural forcings (i.e., solar variability and volcanic aerosols) and anthropogenic forcings (i.e., GHGs and anthropogenic aerosols) (Table 2). The historical GHG (*GHG-forcing*), the historical anthropogenic aerosol (*AA-forcing*), and the historical natural (*NAT-forcing*) simulations are the same as the historical simulations, except that they are only forced by well-mixed GHGs, aerosols, or natural forcings, respectively. All model data are regridded onto a common 2.5° x 2.5° grid with bilinear interpolation. The global land monsoon areas (see definitions below) in the models are masked by the observations.

Table 1. Details of the 5 CMIP5 Models used in this study. All five models include a representation of the direct and indirect aerosol effects.

Model		CanESM2	CSIRO-Mk3-6-0	GFDL-CM3	GISS-E2-H	GISS-E2-R
Institute		CCCma Canada	CSIRO-QCCCE Australia	NOAA-GFDL USA	NASA-GISS USA	NASA-GISS USA
Horizontal resolution		64*128	96*192	90*144	90*144	90*144
Ensemble size	ALL	5	10	5	6	6
	GHG	5	5	3	5	5

	AA	5	5	3	5	5
	Nat	5	5	3	5	5
Natural forcing agents	Solar	SOLARIS	SOLARIS	SOLARIS	SOLARIS	SOLARIS
	Volcanic	S	S	S	S	S
Anthropogenic forcing agents	GHG	IIASA	IIASA	IIASA	IIASA	IIASA
	Aerosol	E1	E2	E1	C	C

SOLARIS: http://sparcsolaris.gfz-potsdam.de/cmip5.php;
S: Sato et al. (1993);
C: The three-dimensional aerosol distributions specified as the monthly 10-year mean aerosol concentrations, derived using the CAM-Chem model, which is driven by the Lamarque et al. (2010); the anthropogenic aerosols include organic carbon (OC), black carbon (BC) and sulfur dioxide (SO_2).
E1: the anthropogenic aerosol emissions taken from the Lamarque et al. (2010);
E2: Same as E1 but with the black carbon increased uniformly by 25% and the organic aerosol increased by 50% (Rotstayn et al. 2012).

Table 2. The list of the CMIP5 control simulations used for evaluating the internal climate variability. The overall drift of the control simulation is removed by subtracting a linear trend over the full period.

No.	Model	Length (year)	Number of non-overlapping 58-year segments non-overlapping 58-year segments
1	bcc-csm1-1	500	8
2	BNU-ESM	559	9
3	CCSM4	501	8
4	CNRM-CM5	600	10
5	CSIRO-Mk3-6-0	500	8
6	CanESM2	996	17
7	FGOALS-g2	900	15
8	GFDL-CM3	500	8
9	GISS-E2-H	480	8
10	GISS-E2-R	850	14
11	HadGEM2-ES	336	5
12	IPSL-CM5A-LR	1000	17
13	MIROC-ESM	531	9

14	MIROC-ESM-CHEM	255	4
15	MRI-CGCM3	500	8
16	NorESM1-M	501	8
17	ACCESS1-0	250	4
18	CESM1-CAM5	319	5
19	FGOALS-s2	501	8
20	HadGEM2-CC	240	4
21	MIROC5	670	11
22	MPI-ESM-LR	1000	17

2.2 Definition of global monsoon region

Global monsoon region is defined as the region with the annual range of precipitation (local summer minus local winter) greater than 2.0 mm day^{-1} and local summer precipitation exceeding 55% of the annual total amount (Wang and Ding., 2008). In the northern (southern) hemisphere, summer (winter) is from May to September, and winter (summer) is from November to March.

2.3 Detection and attribution

According to the IPCC Assessment report, "*Detection of change is defined as the process of demonstrating that climate or a system affected by climate has changed in some defined statistical sense without providing a reason for that change. An identified change is detected in observations if its likelihood of occurrence by chance due to internal variability alone is determined to be small. Attribution is defined as the process of evaluating the relative contributions of multiple causal factors to a change or event with an assignment of statistical confidence.*" (Hegerl et al., 2010; Bindoff et al., 2013; Sun et al., 2013).In the optimal fingerprinting method, observed summer precipitation anomalies averaged over the global land monsoon regions were multi-linearly regressed against the model-based signals via a generalized total least square (TLS) method (Allen and Stott, 2003).

$$y = \sum_{i=1}^{m} \beta_i (x_i - \varepsilon_{x_i}) + \varepsilon_0 \qquad (1)$$

where y represents the observation, x_i represents the climate response to the ith external forcing considered (i.e., the fingerprint or signal of the specific external forcing (e.g., ALL-forcing, GHG-forcing, AA-forcing, or NAT-forcing)). The time series is calculated with five-year non-overlapping averages for the global land monsoon region as a whole. ε_{x_i} represents the effect of internal variability in the estimated responses due to limited number of available simulations. m represents the size of the external forcings. ε_0 represents the noise in the observation and is associated with internal climate variability. β_i is the scaling factor.

Detection of a specific response is claimed if the corresponding scaling factor is significantly inconsistent with zero (i.e., the lower bound of 90% confidence interval of a scaling factor is larger than zero). Furthermore, attribution is claimed if the scaling factor is inconsistent with zero and consistent with one (i.e., the 90% confidence interval includes one), meanwhile other plausible

causes are excluded (Hegerl et al., 2010). The ensemble simulations underestimate (overestimate) the observed response with a β greater (less) than one.

The attributable changes from different external forcings can be further estimated based on the derived scaling factors (e.g., Allen and Stott, 2003; Sun et al., 2014; Xu et al., 2015). For each external forcing, it is estimated as the linear least-square trend from the ensemble mean simulations multiplied by the corresponding scaling factor. The uncertainty ranges of the attributable changes are estimated based on the 90% confidence intervals of β, which involve the effects of internal variability in both observations and simulations.

To estimate the internal variability (i.e., noise), a total of 12489 years in the pi-Control simulations from the 22 CMIP5 models were divided into non-overlapping 58-year chunks, which provided 204 chunks (Table 2). In addition, the intra-ensemble variability (i.e., the residuals of the historical simulations after subtracting their respective ensemble means) was provided for a total of 101 runs (Table 1). For each historical simulation, the period 1890-2005 was used, which provided 2 chunks of the 58-year segments. Thus, 202 chunks of noise estimation were derived from the intra-ensemble variability. In total, the 406 chunks of noise estimation were divided into two independent sets, where one set was used for optimization and the other was used for the residual consistency test (Allen and Tett, 1999; Zhang et al., 2007; Xu et al., 2015).

We conduct the one-signal detection analysis for local summer precipitation changes averaged over the global land monsoon region. The optimal detection is performed in a reduced space spanned by leading empirical orthogonal functions (EOFs) for the model-simulated internal variability (e.g., Zhang et al., 2007; Sun et al., 2014; Xu et al., 2015). The number of EOFs retained is based on the residual consistency test (Allen and Tett, 1999; Allen and Stott, 2003). To test the robustness of the detection results, we perform the detection analysis using a range of numbers of EOFs retained.

2.4 Moisture budget analysis

Within the atmosphere, precipitation is balanced by the sum of evaporation, convergence of the column-integrated moisture flux, and the residual (which mainly includes transient eddies and contributions from surface processes due to topography) (Chou et al., 2013a):

$$P = E - <\nabla \cdot \mathbf{V}q> + \delta \qquad (2)$$

where P represents precipitation, E represents evaporation, $\mathbf{V}$ is the wind vector, q represents the specific humidity, and $-<\nabla \cdot \mathbf{V}q>$ represents the convergence of the column-integrated moisture flux. The term $-<\nabla \cdot \mathbf{V}q>$ can be divided into two terms: vertical moisture advection ($-<\omega \partial_p q>$) and horizontal moisture advection ($-<\mathbf{V}_h \cdot \nabla_h q>$). Then, the changes in precipitation can be expressed by changes in evaporation, horizontal moisture advection, vertical moisture advection, and residuals, as in Eq. (3).

$$P' = E' - <\omega \partial_p q>' - <\mathbf{V}_h \cdot \nabla_h q>' + \delta' \qquad (3)$$

where prime indicates departure from the climatology. The subscripts p and h denote the pressure and the horizontal direction, respectively. $\mathbf{V}_h$ represents the horizontal wind vector, and ∇_h is the horizontal differential operator. The vertical moisture advection change, $-<\omega \partial_p q>'$ is further approximated as the sum of the thermodynamic contribution, $-<\bar{\omega} \partial_p q'>$, the dynamic contribution, $-<\omega' \partial_p \bar{q}>$, and the nonlinear term, $-<\omega' \partial_p q'>$. The overbar denotes the climatology. $-<\bar{\omega} \partial_p q'>$ is associated with changes in water vapor, which are mainly induced by

temperature changes; $-<\omega'\partial_p\bar{q}>$ is associated with changes in pressure velocity, which are mainly induced by atmospheric circulation changes; $-<\omega'\partial_p q'>$ involves changes in both vertical circulation and moisture and is found to be relatively small. Hence, Eq. (3) can be approximated by:

$$P' \approx E' - <\bar{\omega}\partial_p q'> - <\omega'\partial_p\bar{q}> - <\mathbf{V}_h \cdot \nabla_h q>' \qquad (4)$$

Changes in precipitation and evaporation are coupled with each other; thus the causal relationship cannot be distinguished by the moisture budget analysis.

3 Results

3.1 Comparison between observations and model simulations

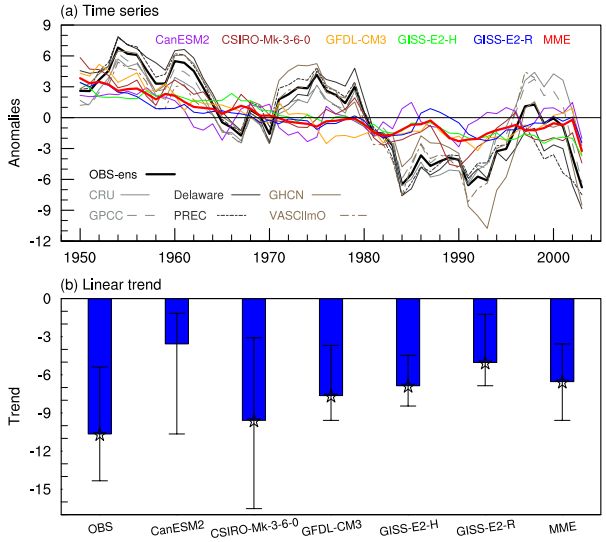

Figure 2. Changes in global land monsoon precipitation during 1948~2005. (a) Time series of local summer precipitation during 1948~2005 averaged over the global land monsoon regions derived from multiple observations and ALL-forcing simulations from the 5 CMIP5 models. Precipitation anomalies (units: mm month^{-1}) are with respect to 1948~2005 and smoothed with a 5-year running mean. The thick black line denotes the multi-observation ensemble mean (without VASClimO due to its shorter time coverage of 1951~2000), and the thick red line denotes the multimodel ensemble mean (MME) of the historical simulations. (b) Linear trends (mm month^{-1} (58yr)$^{-1}$) in local summer precipitation averaged over the global land monsoon regions. Bars represent the ensemble-mean trends, and the error lines show the range of different realizations. Trends that are statistically significant at the 5% level are marked with stars.

We used five sets of observational precipitation data to identify the trends during 1948~2005 in the global land monsoon domain (Fig. 2a). The ensemble mean of the 5 datasets shows a remarkable reduction in monsoon precipitation during the period 1948~2005 (Fig. 2a), with a linear trend of –10.55 (ranging from –5.39 to –14.34) mm month^{-1} (58 yr)$^{-1}$, which corresponds to –5.92% (–3.02% to –8.22%) of the 1961–1990 climatology and is statistically significant at the 1% level (Fig. 2b). The decreasing trend is consistent with previous studies that used more or less data (Wang and Ding, 2006; Zhou et al., 2008a, b; Zhang and Zhou, 2011), demonstrating the robustness of the drying trend.

To estimate the contributions of external forcings, we compare the observed changes to those simulated by the 5 state-of-the-art coupled climate system models of the CMIP5. The 5 models reasonably reproduce the climatology of local summer precipitation over the global land monsoon regions, with a pattern correlation coefficient of 0.84 between the multi-observation ensemble mean and the multimodel ensemble mean (MME), calculated on a common 2.5°×2.5° spatial resolution (only land monsoon regions are retained), forming a solid basis for our analysis of the long term monsoon precipitation changes (Fig. 3a and b).

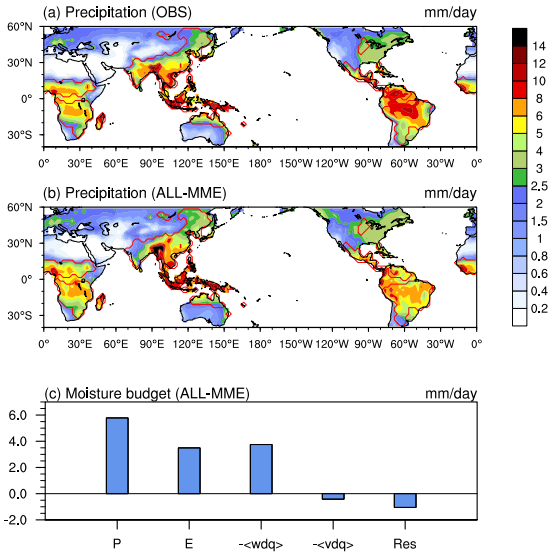

Figure 3. The climatology (units: mm day^{-1}) of the global land summer precipitation in (a) the observations and (b) the MME of the ALL-forcing historical simulations. The red lines denote the global land monsoon region. (c) The climatological moisture budget terms averaged over the global land monsoon region in the MME of the ALL-forcing simulations. P-E is precipitation minus evaporation, $-<wdq>$ is the vertical moisture advection, $-<vdq>$ is the horizontal moisture advection, and Res is the residual term.

In terms of the trends in the local summer precipitation, the all-forcing ensemble (ALL) reasonably captures the drying trend over the global land monsoon domain (Fig. 2a). The drying trend in the MME is –6.49 mm month$^{(-1)}$ (58 years)$^{(-1)}$, or –3.89% of the 1961~1990 climatology, which is within the range of multiple observations (Fig. 2b). All the 5 models are qualitatively consistent in reproducing the drying trend, although with differences in magnitudes. The consistent changes in the local summer global land monsoon precipitation between the observations and the ALL-forcing historical simulations imply that external forcing has played a role in driving the long term changes in the local summer precipitation.

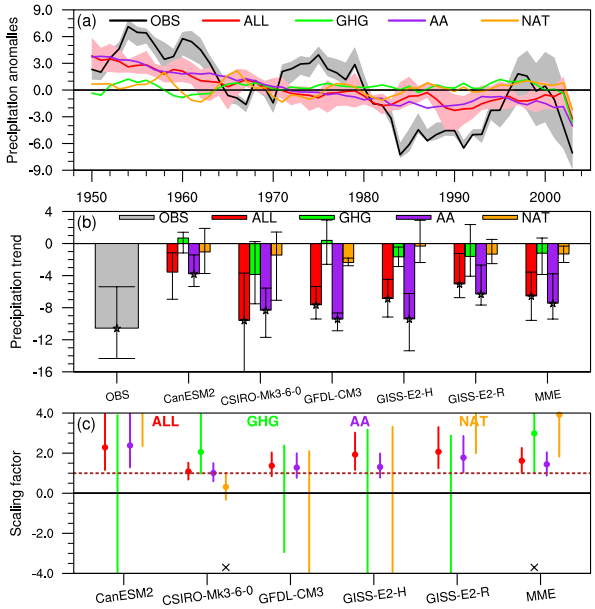

Figure 4. Detection and attribution of global land monsoon precipitation changes under different forcing agents. (a) Time series of the 5-year running average global land monsoon precipitation anomalies with respect to the 1948~2005 mean (units: mm month^{-1}) in the multi-observation ensemble mean and the multimodel ensemble mean under individual forcings. Gray shadings represent the range of different observations, and light pink shadings represent the range of ALL-forcing simulation results. (b) Linear trends (units: mm month^{-1} 58yr^{-1}) in global land monsoon precipitation. Bars represent the ensemble mean, which are labeled with stars if the trend is statistically significant at the 5% level. Error lines represent the ranges of different realizations. (c) The results of the optimal fingerprinting detection at an EOF truncation of 10. Solid circles and error bars represent the best estimate and the 5–95% uncertainty range of the scaling factors, respectively. The cross symbols indicate failure of the residual consistency test at the 10% level. In (a)-(c), red represents ALL-forcing, green represents GHG-forcing, purple represents AA-forcing and orange represents NAT-forcing.

A further comparison of the individual ensembles forced with different forcing combinations reveals that the significant drying trend over the global land monsoon regions originates from anthropogenic influences mainly caused by aerosols (Fig. 4a and b). The dominance of the aerosol forcing on the drying trend is evident in all the 5 models (Fig. 4b). In contrast, the trends of both the GHGs and natural forcing ensembles are weak and statistically insignificant (Fig. 4a and b).

3.2 Detection and attribution of the anthropogenic forcing

The temporal evolutions of the observed and simulated precipitation are compared quantitatively using the "optimal fingerprint" method, a regression procedure that has been widely used in the community of detection studies. We focus on the ensembles of the 5 models. Over the global land monsoon regions, the scaling factors for the ALL-forcing and AA-forcing simulations are significantly greater than zero, indicating that the ALL-forcing and the AA-forcing had a detectable influence on the decrease in global monsoon precipitation. The scaling factors for the ALL-forcing and AA-forcing simulations are consistent with unity, indicating that the decline in global land monsoon precipitation can be attributed to aerosol emissions (Fig. 4c). We note that the detected seasonal mean precipitation changes is different to that of extreme precipitation at regional scales. For example, while the increases in greenhouse gases has had a detectable

contribution to the observed shift toward heavy precipitation in the eastern China, the anthropogenic aerosols partially offset the effect of the greenhouse gases forcing, but cannot be detected by the optimal fingerprint method (Ma et al., 2017).

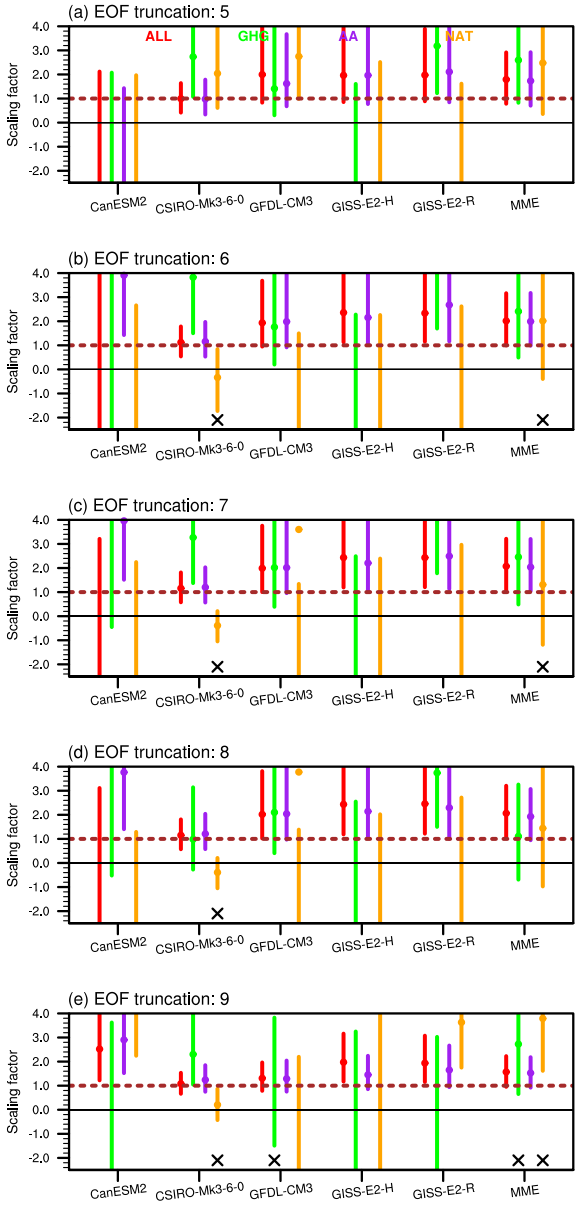

Figure 5. The results of optimal fingerprinting detection at EOF truncations of 5~9. Solid circles and error bars are the best estimate and the 5~95% uncertainty range of scaling factors, respectively. Cross symbols indicate fail of the residual consistency test at the 10% level. The effects of ALL and AA are detectable over a wide range of EOF truncations ranging from 5~10.

The detectable effects of the ALL and AA forcings are consistent in all individual models and over a wide range of EOF truncations ranging from 5~10, demonstrating the robustness of the detection results (Fig. 4c and Fig. 5). The effects of GHG and NAT forcings are not detected, either due to the failure of the residual consistency test or the scaling factor spanning zero, which vary substantially across individual models (Fig. 4c and Fig. 5).

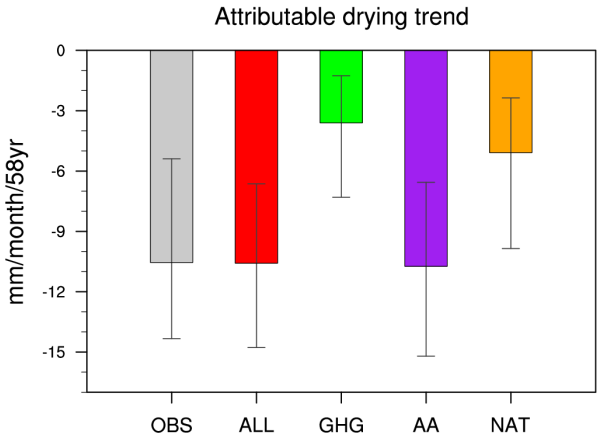

Figure 6. Best estimates of the attributable drying trends due to ALL, GHG, AA, and NAT forcings from the one-signal analysis, along with their 5~95% confidence intervals. For observations (gray bars), the ensemble mean and ranges of multi-observations are shown.

We further estimate the drying trends attributable to different forcing agents by multiplying the simulated linear trends in the MME with respective scaling factors from the one-signal detection analysis (Fig. 6). The ALL forcing has contributed to approximately 100% (63~140% for the 5~95% confidence interval) of the observed trend in the global land monsoon precipitation during 1948~2005 (–10.55 mm month^{-1} (58yr)$^{-1}$). In particular, the anthropogenic aerosols have contributed to 102% (62~144%) of the observed trend.

3.3 Physical processes of difference anthropogenic forcings on precipitation changes

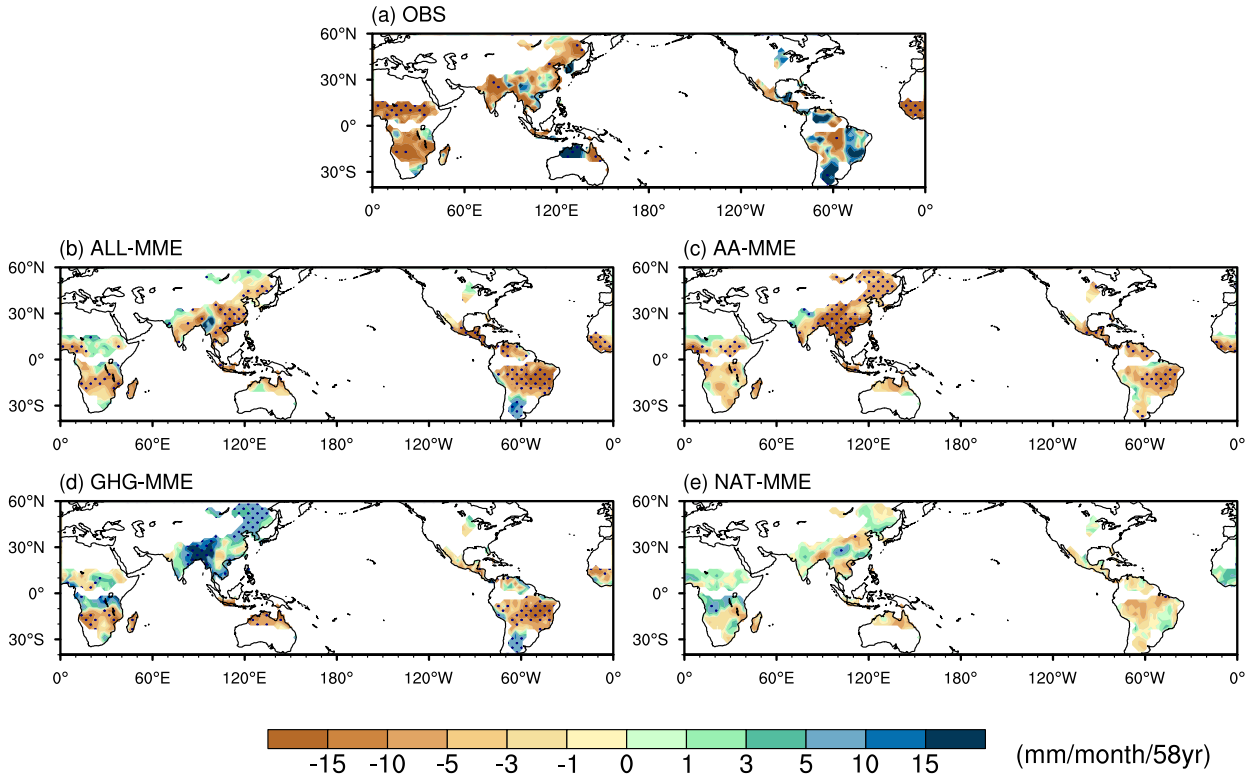

Figure 7. Spatial patterns of linear trends in local summer precipitation under different forcings. The spatial distributions of linear trends in local summer precipitation during 1948~2005 derived from the multi-observation ensemble mean (a), and the multimodel ensemble mean of ALL-forcing simulations (b), AA-forcing simulations (c), GHG-forcing simulations (d), and NAT-forcing simulations (e). Units are mm $month^{-1}$ $(58yr)^{-1}$. Stippling indicates the 5% significance level. Only the global land monsoon regions are shown.

What are the regional features of the monsoon precipitation trends? In the observations, the drying trends are significant in the North and South African monsoon regions, the South and East Asian monsoon regions, part of the Australian monsoon region, and most parts of the North and South American monsoon regions (Fig. 7a). The simulated (ALL-forcing run) large-scale drying trend in precipitation over the global land monsoon regions is generally consistent with the observed pattern, exhibiting more spatially coherent features (Fig. 7b). Regional discrepancies are seen with drying overestimations in the eastern part of the South American monsoon region and underestimations in the eastern part of the North African monsoon region.

Comparisons of the spatial patterns of the precipitation trend under individual forcings confirm the dominant effect of aerosols on the drying trends in the South and East Asian monsoon regions, the North and South American monsoon regions, and part of the African monsoon region (Fig. 7c). The impact of the GHG forcing is more pronounced in the South and East Asian monsoon regions and part of the African monsoon region, leading to wetter conditions (Fig. 7d) and, thus, partly compensating the drying trends caused by aerosols (Fig. 7c). It is worth noting that the GHG forcing has also led to drying conditions in the American monsoon regions (Fig. 7d), which is consistent with simulations driven by an increase in CO_2 due to increased atmospheric stability (Pascale et al., 2017). No significant trends are seen in the natural forcing ensembles (Fig. 7e).

How did the anthropogenic forcings affect the changes in the global land monsoon precipitation? A moisture budget analysis is conducted over the global land monsoon regions during 1948~2005. For the climate mean states, the global land monsoon precipitation is generally balanced by evaporation and vertical moisture advection, whereas the contributions of the horizontal moisture advection and residuals are relatively small and negligible (Fig. 3c).

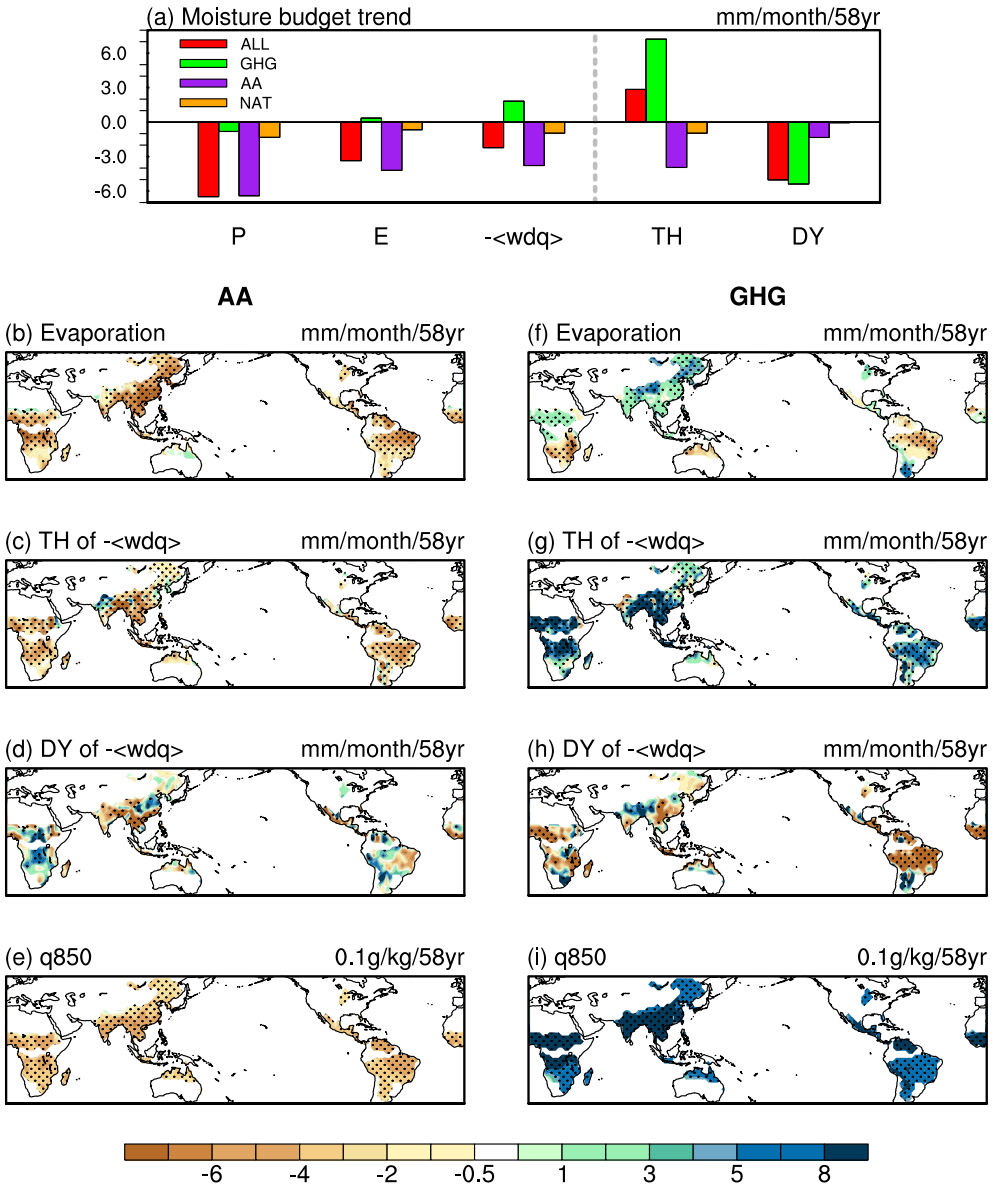

Figure 8. Moisture budget analysis for the drying trend in precipitation. (a) The trends in moisture budget terms averaged over the global land monsoon region. The vertical moisture advection ($-<wdq>$) is separated into a thermodynamic term (*TH*) and a dynamic term (*DY*). The red, green, purple and orange bars denote the MME of the ALL, GHG, AA, and NAT forcings, respectively. (b)-(i) Spatial patterns of linear trends in evaporation (b, f), the thermodynamic (c, g) and dynamic (d, h) terms of the vertical moisture advection, and the specific humidity at 850 hPa (e, i) during 1948~2005 in the multimodel mean of the AA-forcing (b-e) and GHG-forcing (f-i) simulations. Stippling indicates the 5% significance level. Units are mm month^{-1} (58yr)$^{-1}$, except for figures (e) and (i), whose units are 0.1 kg^{-1}(58yr)$^{-1}$.

For the linear trend during 1948~2005 in both the ALL-forcing and AA-forcing experiments, the drying trend in precipitation over the global land monsoon regions is dominated by the vertical

moisture advection, which is further separated into a thermodynamic and dynamic component (Fig. 8a). The thermodynamic increase in moisture advection (higher humidity due to higher temperature) in response to GHG forcing is largely offset by the decrease in the dynamic component (enhanced atmospheric stability and weakening of tropical circulation (Held et al., 2006; Schneider et al., 2010; Chou et al., 2013a, b)). Therefore, the net effect of moisture advection change is weak due to GHG forcing. Both the thermodynamic and dynamic effects of AA cause a reduction in the vertical moisture advection, where the thermodynamic effect is dominant (Fig. 8a).

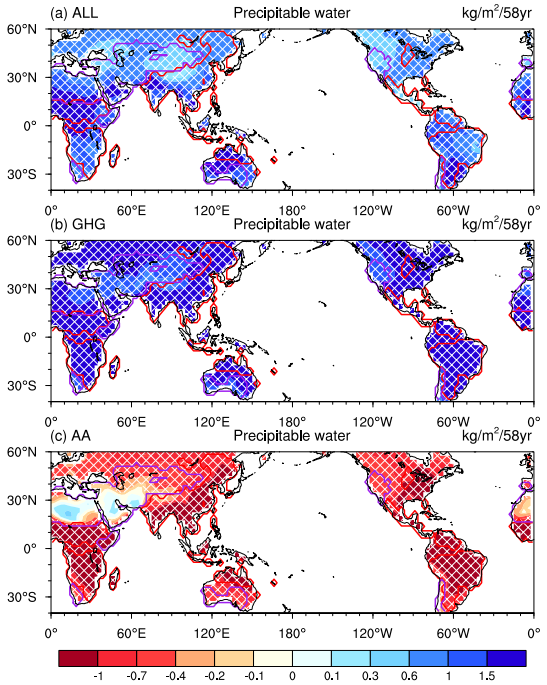

Figure 9. The trends of the precipitable water during the local summer of 1948~2005 for the multi-model ensemble mean of (a) ALL-forcing, (b) GHG-forcing and (c) AA-forcing simulations. The stippling indicates a 10% significance level. The red lines denote the global monsoon regions.

How did the aerosol and GHG changes affect the regional features of monsoon precipitation? For the thermodynamic component of vertical moisture advection, which reduces under the aerosol forcing due to that in specific humidity as the surface cools down, is significant over all land monsoon regions (Fig. 8c and e). In contrast, the GHG forcing increases the specific humidity and hence the thermodynamic component of moisture advection, which is also significant over all land monsoon regions (Fig. 8g and i). The examination of column integrated precipitable water changes shows that the decline in AA-forcing has been offset by an increase in GHG-forcing (Fig. 9). Thus, the thermodynamic effect of GHGs is on par with but opposes the effects of aerosols on precipitation.

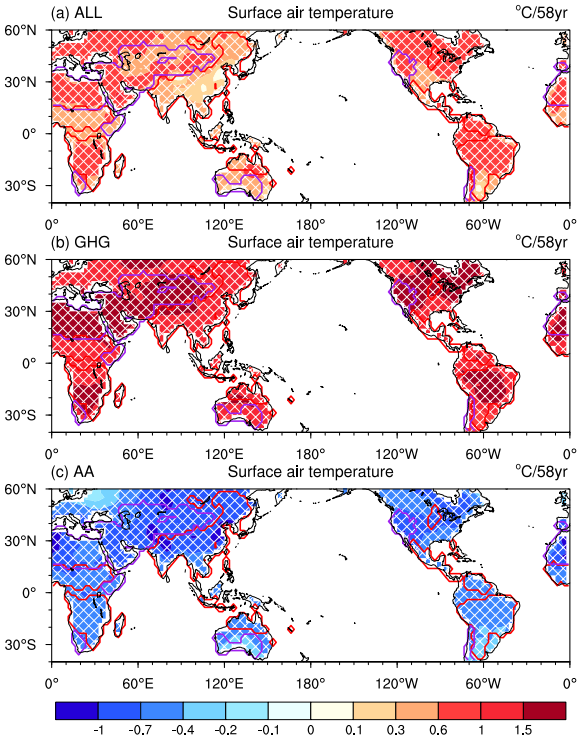

411
412 **Figure 10.** The trends of the surface air temperature during the local summer of 1948~2005 for
413 the multi-model ensemble mean of (a) ALL-forcing, (b) GHG-forcing and (c) AA-forcing
414 simulations. The stippling indicates a 10% significance level. The red lines denote the global
415 monsoon regions.

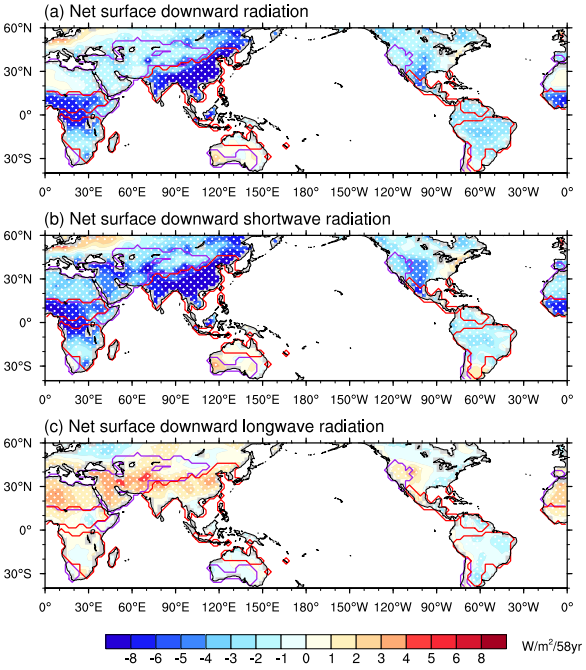

416
417 **Figure 11.** The trends of the (a) net surface downward radiation, (b) net surface downward
418 shortwave radiation, and (c) net surface downward longwave radiation during the local summer of

1948~2005, for the multi-model ensemble mean of the AA-forcing simulations. The stippling indicates a 10% significance level. The red lines denote the global monsoon regions.

Both the GHG-forcing and AA-forcing experiments show a reduction in the dynamic component of moisture advection in the context of globally averaged precipitation over land monsoon regions (Fig. 8a). While the reduction in GHG-forcing is understood to result from increased atmospheric stability and, hence, weakened tropical circulation under global warming (Held et al., 2006; Schneider et al., 2010; Chou et al., 2013b; Lau and Kim, 2017; Pascale et al., 2017), the reduction in AA-forcing results from weakening of the monsoon circulation as a result of the weakened land-ocean thermal contrast and hemispheric asymmetry (i.e., the northern hemisphere is colder than the southern hemisphere (Lau and Kim., 2017)). This is caused by aerosol-induced reductions in downward shortwave radiation through aerosol-radiation and aerosol-cloud interactions (Figs. 10 and 11).

Distinctive regional patterns should be noticed. While the reduction in the dynamic term of the GHG forcing simulation is evident and significant over nearly all land monsoon regions, no well-organized consistent change pattern is seen in the AA-forcing simulation; the reduction is weak and only significant over the Asian monsoon region and parts of the North and South American monsoon regions, while parts of the African monsoon region even witness an increase in precipitation. The dynamic response of regional monsoon circulation to aerosol forcing deserves further study.

4 Conclusions and discussions

In this study, we find that anthropogenic forcing has had a detectable and attributable influence on the significant drying trend of the global land monsoon precipitation during 1948~2005. The optimal fingerprinting analysis shows that the observed drying trend (–10.55 mm month^{-1} (58 yr)$^{-1}$) is attributable to anthropogenic aerosols, with a contribution of 102% (62~144% for the 5~95% confidence interval). A moisture budget analysis reveals that the drying trend in monsoon precipitation results from the reduction in vertical moisture advection due to aerosol forcing. The cooling effects of aerosol forcing are two-fold: a thermodynamic effect due to the reduction in atmospheric humidity and a dynamic effect due to weakening of the land-sea thermal contrast and thus monsoon circulation. Both contribute to the reduction in vertical moisture advection. The warming effects of GHG forcing are also two-fold: a thermodynamic effect, which increases atmospheric moisture, and a dynamic effect, which reduces vertical advection by increasing atmospheric stability. The thermodynamic and dynamic effects largely offset each other, resulting in a weak net wetting trend.

Our demonstration on the effects of anthropogenic aerosol on the drying trend in global monsoon precipitation has important implications for the future. Since much of the monsoon regions, such as India, are also regions of rapid development with increasing aerosol emissions (Li et al., 2016), our results imply that there would be a further reduction in monsoon precipitation in these regions if a clean energy policy is not deployed for effective mitigation in the future. Since the late 1970s, the sulphate aerosol emissions in China has gradually increased, with a decline after 2006 because of adjustment of energy structure in China (Li et al., 2017). The reduction in aerosols emissions not only improved the air quality, but also the water resources in monsoon regions. Given the availability of the monsoon simulation, this study only focused on 1948~2005. Previous studies have shown that the global monsoon precipitation has experienced a recovery since 1979 (Wang et al., 2012; Lin et al., 2014). There is lack of detection and attribution studies to quantify the relative contributions of different external forcings to this increasing trend, although studies

indicated that the anthropogenic greenhouse gases may play a role (Wang et al., 2012; Zhang and Zhou, 2014).

Although we used ensemble simulations from CMIP5, particularly multi-model and members, to increase the robustness of the results, we note that there are still large uncertainties in the estimatation of aerosol forcing on precipitation changes due to the complexity of aersol climate effects, including the direct and indirect effects of aerosols (Wu et al., 2018; Li et al., 2016; Zhou et al., 2018). Limited observational and cloud-resolving modeling studies suggest that the net effect (enhance or suppress) of aerosol on precipitation relies on the aerosol type, meteorological background (such as cloud-water content), precipitation intensity, region of interest, etc. (Zhao et al., 2006; Qian et al., 2009; Li et al., 2011). The aerosol satellite observations and stational precipitation observations show that the increase in aerosol concentration in China during the past several decades can increase the atmospheric stability, weaken vertical motion and reduce total rainfall over eastern China (Zhao et al., 2006). Aerosols can also increase cloud droplet number concentration, reduce the cloud droplet size and thus contribute to the decreasing trend in light rainfall over easten China (Qian et al., 2009). In addition, the quality of aerosol forcing in each monsoon region used to force the historical simulations exists large uncertainty. There is substantial uncertainty in present-day top-of-atmosphere aerosol effective radiative forcing, with a 5%-to-95% confidence interval spanning –1.9 W m^{-2} to –0.1 W m^{-2} (Myhre et al., 2013). The uncertainty in aerosol radiative forcing is one of the uncertainty sources for detection and attribution results and the associated physical understanding. The undergoing sixth phase of Coupled Model Intercomparison Project (CMIP6, Eyring et al., 2016) updated the historical anthorogenic aerosol forcing, greenhouse gas forcing and land use forcing, which are used for the Detection and Attribution Model Intercomparison Project (DAMIP, Gillett et al., 2016). The new output would provide solid data support for the attribution studies of monsoon precipitation changes. It is desirable to examine the monsoon precipitation response to aersol forcing based on the newly released CMIP6 output. We should note that the multi-model framework of CMIP may also include structural or parametric uncertainties. It remains a challenge in the climate research community as to improve the model simulation of the aerosol-monsoon interaction, and to reduce uncertainties in aerosol-climate feedback based on observations (Li et al., 2011; Wu et al., 2015; Zhou et al., 2018).

Acknowledgments

This work is jointly supported by the CAS Strategic Priority Research Program (XDA20060102), China MOST program (2018YFC1507701) and the National Natural Science Foundation of China (Grant Nos. 41775091). Yun Qian's contribution is supported as part of the Energy Exascale Earth System Model (E3SM) project, funded by the U.S. Department of Energy, Office of Science, Office of Biological and Environmental Research. The Pacific Northwest National Laboratory (PNNL) is operated for DOE by Battelle Memorial Institute under contract DE-AC06-76RLO 1830. We also acknowledge the support from Jiangsu Collaborative Innovation Center for Climate Change. The CMIP5 simulations used in this paper can be accessed from https://esgf-node.llnl.gov/search/cmip5/. Observational precipitation datasets for GPCC, University of Delaware, PREC/L, and GHCN are available from https://www.esrl.noaa.gov/psd/data/, while for CRU is from https://crudata.uea.ac.uk/cru/data/precip/, and for VASClimO is from http://iridl.ldeo.columbia.edu/SOURCES/.DEKLIM/.VASClimO/.PrcpClim/#info.

References

Allen M and Tett S. 1999. Checking for model consistency in optimal fingerprinting. Clim Dynam, 15(6): 419−434.

Allen M and Stott P 2003. Estimating signal amplitudes in optimal fingerprinting, Part I: Theory. Clim Dynam, 21(5-6), 477−491.

Annamalai H, Hafner J, Sooraj K, Pillai P. 2013 Global warming shifts the monsoon circulation, drying South Asia. J Clim, 26: 2701–2718. https://doi.org/10.1175/JCLI-D-12-00208.1

Beck C, Grieser J and Rudolf B. 2005. A new monthly precipitation climatology for the global land areas for the period 1951 to 2000. DWD, Klimastatusbericht KSB 2004, ISSN 1437-7691, ISSN 1616-5063 (Internet), ISBN 3-88148-402-7, 181−190.

Bindoff N, Stott P, AchutaRao K, Allen M, Gillett N, Gutzler D, Hansingo K, Hegerl G, Hu Y, Jain S, Mokhov I, Overland J, Perlwitz J, Sebbari R and Zhang X, 2013. Detection and attribution of climate change: from global to regional. In: Climate Change 2013: The Physical Science Basis. Contribution of Working Group I to the Fifth Assessment Report of the Intergovernmental Panel on Climate Change. Stocker, T.F., D. Qin, G.-K. Plattner, M. Tignor, S.K. Allen, J. Boschung, A. Nauels, Y. Xia, V. Bex and P.M. Midgley eds.. Cambridge : Cambridge University Press. 86.

Bollasina M, Ming Y and Ramaswamy V. 2011. Anthropogenic aerosols and the weakening of the South Asian summer monsoon. Science, 334(6055): 502−505.

Chen M, Xie P, Janowiak J, and Phillip A. 2002. Global land precipitation: A 50-yr monthly analysis based on gauge observations. J. Hydrometeor. 3(3): 249−266.

Chen X and Zhou T. 2015. Distinct effects of global mean warming and regional sea surface warming pattern on projected uncertainty in the South Asian summer monsoon. Geophys Res Lett, 42(21): 9433−9439.

Chou C, Wu T and Tan P. 2013a. Changes in gross moist stability in the tropics under global warming. Clim Dynam, 41(9-10):2481−2496.

Chou C, Chiang J, Lan C, Chung C, Liao Y, Lee C. 2013b. Increase in the range between wet and dry season precipitation. Nat Geosci, 6(4): 263−267.

Dong B, Sutton R, Highwood E, Wilcox L. 2016. Preferred response of the East Asian summer monsoon to local and non-local anthropogenic sulphur dioxide emissions. Clim Dyn, 46:1733−1751. doi:10.1007/s00382-015-2671-5.

Eyring V, Bony S, Meehl G A, Senior C A, Stevens B, Stouffer R J, and Taylor K E. 2016. Overview of the Coupled Model Intercomparison Project Phase 6 (CMIP6) experimental design and organization, Geosci Model Dev, 9: 1937–1958, doi:10.5194/gmd-9-1937-2016.

Gillett N, Shiogama H, Funke B, Hegerl G, Knutti R, Mattes K, Santer B, Stone D, Tebaldi C. 2016. The Detection and Attribution Model Intercomparison Project (DAMIP v1.0) contribution to CMIP6. Geoscientific Model Development, 9:3685−3697.

Guo L, Highwood E, Shaffrey L and Turner A. 2013. The effect of regional changes in anthropogenic aerosols on rainfall of the East Asian Summer Monsoon. Atmospheric Chem Phys. 13(3):1521−1534.

Harris I, Jones P, Osborn T and Lister D. 2014. Updated high-resolution grids of monthly climatic observations – the CRU TS3.10 Dataset. Int J Climatol, 34(3): 623−642.

Held I, Delworth T, Lu J, Findell K. and Knutson T. 2005. Simulation of Sahel drought in the 20th and 21st centuries. Proc. Natl Acad. Sci. 102(50): 17891−17896.

Held I and Soden B. 2006. Robust responses of the hydrological cycle to global warming. J Clim,

19(21): 5686−5699.
Hegerl G, Hoegh-Guldberg O, Casassa G, Hoerling M, Kvats S, Parmesan C, Pierce D, Stott P. 2010. Good practice guidance paper on detection and attribution related to anthropogenic climate change. In: Meeting Report of the Intergovernmental Panel on Climate Change Expert Meeting on Detection and Attribution of Anthropogenic Climate Change. T. F. Stocker, et al. eds.. IPCC Working Group I Technical Support Unit, University of Bern, Bern, Switzerland, 8.
Huang X, Zhou T, Turner A, Dai A, Chen X, Clark R, Jiang J, Man W, Murphy J, Rostron J, Wu B, Zhang L, Zhang W, Zou L. 2020. The Recent decline and recovery of Indian summer monsoon rainfall: relative roles of external forcing and internal variability. J Clim, https://doi.org/10.1175/JCLI-D-19-0833.1
Jiang J, Zhou T. 2019. Global monsoon responses to decadal sea surface temperature variations during the twentieth century: Evidence from AGCM simulations. J Clim, 32: 7675−7695. doi: 10.1175/JCLI-D-18-0890.1
Jiang Y, Liu X, Yang X Q, Wang M. 2013. A numerical study of the effect of different aerosol types on East Asian summer clouds and precipitation, Atmospheric Environment, 70: 51−63, doi: 10.1016/j.atmosenv.2012.12.039.
Jiang Y, Yang X Q, and Liu X. 2015. Seasonality in anthropogenic aerosol effects on East Asian climate simulated with CAM5, Journal of Geophysical Research – Atmospheres, 120: 10837−10861, doi: 10.1002/2015JD023451
Kitoh A, Endo H, Kumar K, Cavalcanti I, Goswami P, Zhou T. 2013. Monsoons in a changing world: a regional perspective in a global context. J Geophys Res, 118(8): 3053−3065.
Krishnan R, Sabin T, Vellore R, Mujumdar M, Sanjay J, Goswami B, Hourdin F, Dufresne J, Terray P. 2016. Deciphering the desiccation trend of the South Asian monsoon hydroclimate in a warming world. Climate Dynamics, 47 (3):1007−1027.
Krushnamurthy L and Krishnamurthy V. 2014. Influence of PDO on South Asian summer monsoon and monsoon–ENSO relation. Climate Dynamics, 42: 2397−2410.
Lamarque J, Bond T, Eyring V, Granier C, Heil A, Klimont Z, Lee D, Liousse C, Mieville A, Owen B, Schultz M, Shindell D, Smith S, Stehfest E, J. Van Aardenne, Cooper O, Kainuma M, Mahowald N, McConnell J, Naik V, Riahi K, and van Vuuren D. 2010. Historical (1850-2000) gridded anthropogenic and biomass burning emissions of reactive gases and aerosols: Methodology and application, Atmos Chem Phys, 10: 7017−7039.
Lau K, Kim M and Kim K. 2006. Asian summer monsoon anomalies induced by aerosol direct forcing: the role of the Tibetan Plateau. Clim Dynam, 26(7-8): 855−864.
Lau W and Kim K. 2017. Competing influences of greenhouse warming and aerosols on Asian summer monsoon circulation and rainfall. Asia-Pac J Atmospheric Sci, 53(2): 181−194.
Li H, Dai A, Zhou T. and Lu J. 2010. Responses of East Asian summer monsoon to historical SST and atmospheric forcing during 1950–2000. Clim Dynam, 34(4): 501−514.
Li M, Liu H, Geng G, Hong H, Liu F, Song Y, Tong D, Zheng B, Cui H, Man H, Zhang Q, He K. 2017. Anthropogenic emission inventories in China: a review. National Science Review, 4: 834−866, 2017, doi: 10.1093/nsr/nwx150
Li Z, Lau W, Ramanathan V, Wu G, Ding Y, Manoj M, Liu J, Qian Y, Li J, Zhou T, Fan J, Rosenfeld D, Ming Y, Wang Y, Huang J, Wang B, Xu X, Lee S, Cribb M, Zhang F, Yang X, Zhao C, Takemura T, Wang K, Xia X, Yin Y, Zhang J,Guo J, Zhai P, Sugimoto N, Babu S, Brasseur G. 2016. Aerosol and monsoon climate interactions over Asia. Rev Geophys, 54 (4): 866−929.

Li Z. Li C, Chen H, Tsay S, Holben B, Huang J, Li B, Maring H, Qian Y, Shi G, Xia X, Yin Y, Zheng Y, Zhuang G. 2011. East Asian studies of tropospheric aerosols and their impact on regional climate (EASTAIRC): an overview, J Geophys Res, 116, D00K34, doi:10.1029/2010JD015257.

Lin R, Zhou T, Qian Y. 2014. Evaluation of global monsoon precipitation changes based on five reanalysis datasets, J Clim, 27(3): 1271−1289,doi: http://dx.doi.org/10.1175/JCLI-D-13-00215.1

Meehl G, Arblaster J and Collins W. 2008. Effects of black carbon aerosols on the Indian monsoon. J Clim, 21(12): 2869−2882.

Ma S, Zhou T, Stone D, Polson D, Dai A, Stott P, Storch H, Qian Y, Burke C, Wu P, Zou L, and Ciavarella A. 2017: Detectable anthropogenic shift toward heavy precipitation over eastern China. J Clim, 30: 1381−1396, doi:10.1175/JCLI-D-16-0311.1.

Myhre G, Shindell D, Bréon F M, Collins W, Fuglestvedt J, Huang J, et al. 2013. Anthropogenic and natural radiative forcing – in Climate Change 2013: the Physical Science Basis. Contribution of Working Group I to the Fifth Assessment Report of the Intergovernmental Panel on Climate Change. Cambridge University Press, https://doi.org/10.1017/CBO9781107415324

Pascale S, Boos W, Bordoni S, Bordoni S, Delworth T, Kapnick S, Murakami H, Vecchi G, Zhang W. 2017. Weakening of the North American monsoon with global warming. Nat Clim Change, 7(11): 806.

Paul S, Ghosh S, Oglesby R, Pathak A, Chandrasekharan A, Ramsankaran R. 2016 Weakening of Indian summer monsoon rainfall due to changes in land use land cover. Sci Rep, 6:32177.

Peterson T and Vose R. 1997. An overview of the Global Historical Climatology Network temperature database. Bull Am Meteorol Soc, 78(12): 2837−2849.

Polson D, Bollasina M, Hegerl G and Wilcox L. 2014. Decreased monsoon precipitation in the Northern Hemisphere due to anthropogenic aerosols. Geophys Res Lett, 41(16): 6023–6029.

Rotstayn L, Jeffrey S, Collier M, Dravitzki S, Hirst A, Syktus J andWong K. 2012. Aerosol- and greenhouse gas-induced changes in summer rainfall and circulation in the Australasian region: a study using single-forcing climate simulations, Atmos Chem Phys, 12: 6377−6404.

Salzmann M, Weser H, Cherian R. 2014. Robust response of Asian summer monsoon to anthropogenic aerosols in CMIP5 models. Journal of Geophysical Research: Atmospheres, 119 (19):11321−311337.

Qian Y, Flanner M, Leung L & Wang W. 2011. Sensitivity studies on the impacts of Tibetan Plateau snowpack pollution on the Asian hydrological cycle and monsoon climate. Atmospheric Chem Phys, 11(5): 1929−1948.

Qian Y, Gong D Y, Fan J W, Leung L R, Bennartz R, Chen D L, Wang W G. 2009. Heavy pollution suppresses light rain in China: Observations and modeling. J Geophys Res, 114: D00K02, doi: 10.1029/2008JD011575

Sato M, Hansen J, McCormick M, and Pollack J. 1993. Stratospheric aerosol optical depths, J Geophys Res, 98: 22987−22994.

Schneider T, O'Gorman P and Levine X. 2010. Water vapor and the dynamics of climate changes. Rev Geophys, 48, RG3001, https://doi.org/10.1029/2009RG000302.

Schneider U, Becker A, Finger P, Meyer-Christoffer A, Ziese M, and Rudo B. 2014. GPCC's new land surface precipitation climatology based on quality-controlled in situ data and its role

in quantifying the global water cycle. Theor Appl Climatol, 115(1-2): 15−40.
Song F, Zhou T and Qian Y. 2014. Responses of East Asian summer monsoon to natural and anthropogenic forcings in the 17 latest CMIP5 models. Geophys Res Lett, 41(2): 596–603.
Sun Y, Zhang X, Zwiers F, Song L, Wan H, Hu T, Yin H, Ren G. 2014. Rapid increase in the risk of extreme summer heat in Eastern China. Nature Climate Change, 4(12): 1082.
Sun Y, Yin H, Tian Q, Hu T, Shi Y, Liu H, Zhou B. 2013. Recent progress in studies of climate change detection and attribution in the globe and China in the Past 50 years. Climate Change Research (in Chinese), 9(4): 235−245.
Taylor K E, Stouffer R J and Meehl G A. 2012. An overview of CMIP5 and the experiment design. Bull Am Meteorol Soc, 93: 485−498.
Wang B, Ding Q. 2006. Changes in global monsoon precipitation over the past 56 years. Geophys Res Lett, 33：L06711. doi:10.1029/2005GL025347
Wang B, Ding Q. 2008. Global monsoon: Dominant mode of annual variation in the tropics. Dynamics of Atmospheres and Oceans, 44(3-4): 165–183.
Wang B, Liu J, Kim H, Webster P and Yim S. 2012. Recent change of the global monsoon precipitation (1979–2008). Clim Dynam, 39(5): 1123−1135.
Wang B, Liu J, Kim HJ, Webster PJ, Yim SY, Xiang B. 2013. Northern Hemisphere summer monsoon intensified by mega-El Nino/southern oscillation and Atlantic multidecadal oscillation. Proc Natl Acad Sci, 110 (14):5347−5352.
Wang Z, Lin L, Yang M, Xu Y, Li J. 2017. Disentangling fast and slow responses of the East Asian summer monsoon to reflecting and absorbing aerosol forcings. Atmos Chem Phys, 17 (18): 11075−11088, doi:10.5194/acp-17-11075-2017.
Willmott C, Matsuura K. 2001. Terrestrial air temperature and precipitation: Monthly and annual time series (1950-1996). http://climate. geog. udel. edu/~ climate/html_pages/README. ghcn_ts. html.
Wu G, Li Z, Fu C, Zhang X, Zhang R Y, Zhang R H, Zhou T, Li J, Li J, Zhou D, Wu L, Zhou L, He B & Huang R. 2015. Advances in studying interactions between aerosols and monsoon in China. Sci China Earth Sci (in Chinese), 45: 1−19. doi:10.1007/s11430-015-5198-z
Wu P, Christidis N, and Stott P. 2013. Anthropogenic impact on Earth's hydrological cycle. Nat Clim Change, 3(9): 807−810.
Xu Y, Gao X, Shi Y, Zhou B. 2015. Detection and attribution analysis of annual mean temperature changes in China. Climate Research, 63(1): 61−71.
Yang X, Zhu Y, Xie Q, Ren X, and Xu G. 2004. Advances in studies of Pacific Decadal Oscillation. Chinese Journal of Atmospheric Sciences (in Chinese), 28(6): 979−992.
Zhang L and Zhou T. 2011. An assessment of monsoon precipitation changes during 1901–2001. Clim Dynam, 37(1-2): 279−296.
Zhang L and Zhou T. 2014. An Assessment of Improvements in Global Monsoon Precipitation Simulation in FGOALS-s2?, Advances in Atmospheric Sciences, 31(1): 165−178, doi: 10.1007/s00376-013-2164-6.
Zhang W, Zhou T, Zou L, Zhang L, and Chen X. 2018. Reduced exposure to extreme precipitation from 0.5C less warming in global land monsoon regions. Nature Communications. 9: 3153. doi:10.1038/s41467-018-05633-3
Zhang X, Zwiers F W, Hegerl G. C., et al. 2007. Detection of human influence on twentieth-century precipitation trends. Nature, 448(7152): 461.
Zhao C, Tie X, and Lin Y. 2006. A possible positive feedback of reduction of precipitation and increase in aerosols over eastern central China, Geophys Res Lett, 33, L11814,

694 doi:10.1029/2006GL025959.
695 Zhou T, Zhang L and Li H. 2008a. Changes in global land monsoon area and total rainfall
696 accumulation over the last half century. Geophys Res Lett, 35(16).
697 Zhou T, Yu R, Li H, Wang B. 2008b. Ocean forcing to changes in global monsoon precipitation
698 over the recent half-century. J Clim, 21(15): 3833−3852.
699 Zhou T, Wu B, Guo Z, He C, Zou L, Chen X, Zhang L, Man W, Li P, Li D, Yao J, Huang X, Zhang
700 W, Zuo M, Lu J, Sun N. 2018. A review of East Asian summer monsoon simulation and
701 projection: Achievements and problems, opportunities and challenges. Chinese Journal of
702 Atmospheric Sciences (in Chinese), 42 (4): 902−934, doi:10.3878/j.issn.1006-
703 9895.1802.17306.
704 Zhu Y, Yang X. 2003. Relationships between Pacific Decadal Oscillation and climate variabilities
705 in China. Acta Meteorologica Sinica (in Chinese), 61(6):641−654.
706